

A Scalable Protocol for Cooperative Time Synchronization Using Spatial Averaging

An-swol Hu

Sergio D. Servetto

Abstract—Time synchronization is an important aspect of sensor network operation. However, it is well known that synchronization error accumulates over multiple hops. This presents a challenge for large-scale, multi-hop sensor networks with a large number of nodes distributed over wide areas. In this work, we present a protocol that uses spatial averaging to reduce error accumulation in large-scale networks. We provide an analysis to quantify the synchronization improvement achieved using spatial averaging and find that in a basic cooperative network, the skew and offset variance decrease approximately as $1/\bar{N}$ where \bar{N} is the number of cooperating nodes. For general networks, simulation results and a comparison to basic cooperative network results are used to illustrate the improvement in synchronization performance.

I. INTRODUCTION

A. Synchronization and the Scalability Problem

Many synchronization techniques have been proposed for synchronizing sensor networks [1], [2], [3], [4], [5]. These techniques all rely on nodes exchanging packets with timing information. Using the exchanged timing information, each node can then estimate clock offset and maybe clock skew. However, all of these traditional synchronization techniques suffer from an inherent scalability problem—synchronization error accumulates over multiple hops. At each hop, nodes will estimate synchronization parameters, but the estimates will have errors. Therefore, when these erroneous parameters are used to communicate timing information to the next hop, errors will further increase.

This accumulation of error over multiple hops poses a problem as sensor networks are deployed over larger and larger areas. The number of hops required to communicate across the network increases and, thus, the synchronization error across the network increases as well. One possible way to avoid the scalability problem is to use a few nodes with powerful radios to limit the number of hops required to communicate timing information across the network. However, this technique does not address the fundamental scalability problem of errors accumulating over multiple hops.

In this work, we consider the use of high density networks to mitigate the scalability problem. Recent developments [6], [7], [8] suggest that future networks may have extremely large numbers of nodes deployed over wide areas. The question we consider is whether or not the density of future networks can be used to address scalability issues that plague existing techniques.

The authors are with the School of Electrical and Computer Engineering, Cornell University, Ithaca, NY. URL: <http://cn.ece.cornell.edu/>. Work supported by the National Science Foundation, under awards CCR-0238271 (CAREER), CCR-0330059, and ANR-0325556.

B. Motivation for Cooperation

In order to reduce the scalability problem, we need to find ways to reduce the synchronization error at each hop. There are two primary ways to accomplish this. The first is to collect more timing information. With more timing data, nodes can generally make a better estimate of clock skew and clock offset. For example, RBS and FTSP both let nodes collect many timing data points before estimating clock skew and clock offset. A timing data point provides a node with the time at a reference clock at a specific time in its local time scale. With more data points, synchronization error will decrease. This idea is essentially doing a *time* average to estimate clock skew and clock offset. However, this is not necessarily practical since it would significantly increase the time to synchronize and the amount of network traffic.

The second primary approach is to improve the quality of the timing data point. For example, TPSN and FTSP use MAC layer time stamping techniques that are more accurate. However, we believe that there is a fundamentally new technique for improving data point quality that has not been considered before. This new idea is to use spatial averaging to improve data point quality. In a high density network, we have a large number of surrounding nodes. Instead of only doing a time average to estimate the clock skew and clock offset, perhaps we can also do a *spatial* average to improve these estimates.

C. Approach to Cooperation

We assume the network is setup such that one node, called node 1, has the reference clock that all other nodes want to synchronize to. Node 1 will communicate timing information to the nodes in its broadcast domain, the R_2 nodes. The R_2 nodes will then communicate timing information to the nodes that are another hop out, the R_3 nodes. This process continues until all nodes are synchronized (Fig. 1).

Each node in R_i , $i \geq 1$, will use information from the R_{i-1} nodes to estimate its clock skew and clock offset. With these parameters, the node will be able to send a sequence of m pulses that are approximately d seconds apart in the reference time scale, where d and m are pre-specified by the protocol. All nodes in the R_i set will be attempting to send pulses at the same time. However, due to synchronization error, the pulses will only be occurring at approximately the same time. Thus, any node in the R_{i+1} set of nodes will observe m clusters of pulses instead of just m individual pulses.

Since each pulse in a cluster represents one R_i node's attempt to transmit at some appropriate time in the reference time scale, taking the sample mean of the pulse arrival times in

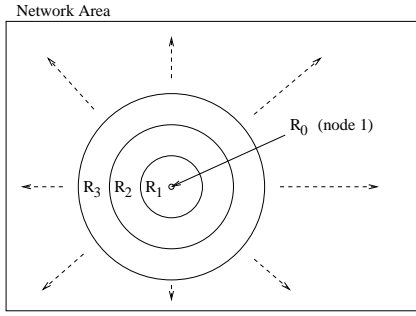


Fig. 1. For increasing i , the R_i nodes are progressively farther and farther away from reference node 1, the R_0 node. Each node in the set R_i receives its timing information from a group of nodes in R_{i-1} .

each cluster allows us to average out some of the error made by any one node in R_i . The process of having each node in R_{i+1} use the sample mean of each cluster as a timing data point is the key to spatial averaging. Since each R_{i+1} node can use timing information from many surrounding neighbors in R_i , we call our technique *cooperative time synchronization*. Using these timing data points, and some additional information from the R_i set, every node in R_{i+1} can estimate its clock skew and offset. Thus, this process can then repeat to synchronize the R_{i+2} nodes.

The difficulty in studying this problem is that, generally, the m clusters observed by any particular node in R_{i+1} will be different from the m clusters observed by any other node in R_{i+1} . This is because the clusters observed by a node will depend on where this node is located relative to the R_i set of nodes. Therefore, to study how cooperation can improve synchronization, we approach the problem in two steps.

First, we set up a basic cooperative network (Type I network) that is a base case for cooperation. The key assumption in a Type I network is that all nodes in R_{i+1} are in the broadcast domain of all nodes in R_i . Note that this is a generalization of the non-cooperative situation where timing information is passed from one node to the next. Fig. 2 compares the basic cooperative network to a non-cooperative network. With the Type I network we analytically quantify how the variance of the skew and offset estimates grow with increasing hop number.

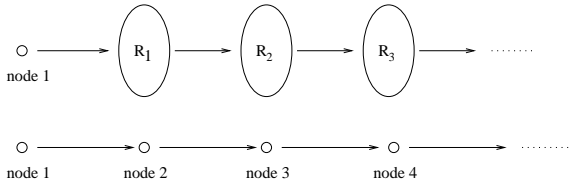


Fig. 2. Top: A basic cooperative network (Type I network) where timing information is communicated from the R_i set of nodes to the R_{i+1} set. This Type I deployment assumes many nodes in each R_i set. Bottom: Assuming each R_i set has only one node, we have the non-cooperative situation.

Second, we use the theoretical results from the basic cooperative network to understand the behavior of a general Type II network where nodes are uniformly distributed over a circular area. Simulation results are used to illustrate that increasing

network density improves synchronization performance.

D. Other Related Work

The traditional synchronization techniques describe in [1], [2], [3], [4], [5] all operate fundamentally on the idea of communicating timing information from one set of nodes to the next. One other approach to synchronization that has recently received much attention is to apply mathematical models of natural phenomena to engineered networks. A model for the emergence of synchrony in pulse-coupled oscillators was developed in [9] for a fully-connected group of identical oscillators. In [10], this convergence to synchrony result was extended to networks that were not fully connected.

The convergence result is clearly desirable for synchronization in networks and in [11] theoretical and simulation results suggested that such a technique could be adapted to communication and sensor networks. Experimental validation for the ideas of [9] was obtained in [12] where the authors implemented the Reachback Firefly Algorithm (RFA) on TinyOS-based nodes.

The problem with these emergent synchronization results is that the fundamental theory assumes all nodes have nearly the same firing period. Results from [11] and [12] show that the convergence results may hold when nodes have approximately the same firing period, but the authors of [12] explain that clock skew will degrade synchronization performance. Since we are not aware of any results that provide an extension to deal with networks of nodes with arbitrary firing periods, our work focuses on synchronization algorithms that explicitly estimate clock skew.

E. Contributions and Paper Organization

In this paper, we propose a protocol for time synchronization that uses spatial averaging to improve synchronization performance. In this work we make the following analysis:

- 1) Mathematically quantify the synchronization error for the Type I basic cooperative network.
- 2) Through simulations, show that increasing node density can decrease synchronization error in general networks.

The results show that if each node can hear a large number of neighboring nodes, then nodes can cooperatively generate signals that are less noisy and allow for better synchronization performance over multiple hops. The fact that more cooperating nodes yields better performance means that there exists a new trade-off between network density and synchronization performance where more nodes provide better synchronization. Even though it is possible to achieve better synchronization performance by introducing nodes with powerful radios to synchronize a large-scale network, cooperative time synchronization is an effective alternative technique to reducing synchronization error across the network without requiring special nodes.

The remainder of the paper is organized as follows. In Section II we set up the general network assumptions and present the synchronization protocol in Section III. The analysis and simulations of the protocol for a basic cooperative network are

presented in Section IV while a study of cooperation in general networks is carried out in Section V. We make concluding remarks in Section VI.

II. SYSTEM MODEL

A. Clock Model

The behavior of each node i is governed by a clock c_i that counts up from 0. The introduction of c_i is important since it provides a consistent timescale for node i . This is the node's local time scale and in synchronization the node tries to estimate how its local clock is related to the reference clock.

We assume that node 1 contains the reference clock and every node in the network is to be synchronized to this clock. The clock of node 1, c_1 , will be defined as $c_1(t) = t$ where $t \in [0, \infty)$. We now define the clock of any other arbitrary node i , c_i , as

$$c_i(t) = \alpha_i(t - \bar{\Delta}_i) + \Psi_i(t), \quad (1)$$

where

- $\bar{\Delta}_i$ is an unknown offset between the start times of c_i and c_1 .
- $\alpha_i > 0$ is an unknown constant for each i .
- $\Psi_i(t)$ is a stochastic process modelling random timing jitter. $\Psi_i(t)$ is a zero mean Gaussian process with independent and identically distributed Gaussian samples with mean zero and variance σ^2 , i.e. $\mathcal{N}(0, \sigma^2)$. We assume $\sigma^2 < \infty$ and note that σ^2 is defined in terms of the clock of node i .

Note that this linear relationship is valid for short periods of time since we do not explicitly model clock drift.

B. Transmission Model

Each node i in the network can transmit short pulses $p(t)$ for time synchronization. These are short duration pulses, i.e. ultra wideband pulses, and for our purposes we consider them to be delta functions $\delta(t)$. The particular choice of $p(t)$ is not important. For the purposes of studying cooperative time synchronization, we assume a node receiving the pulse can uniquely determine a pulse arrival time, pulses sent from different nodes do not overlap, and a node seeing multiple pulses can identify the different pulse arrival times. Note that only minor modifications of the protocol are needed to accommodate other types of pulse shapes [14].

We assume that each node has a transmission range of R . This means that a node j must be within a distance R from a transmitting node i in order to hear pulses from node i . Note that the assumption of a circular transmission region is made only to simplify the illustration of spatial averaging. The synchronization protocol proposed in Section III does not require this assumption and most of the results in this work will hold under more realistic conditions [15], [16]. Since we are dealing with sensor nodes who have short transmission distances, we further assume that propagation delay is negligible. We make this assumption since from [5] we know that propagation delay is less than $1\mu\text{s}$ for distances up to 300 meters. Some results on cooperation and propagation delay are available in [13].

III. SYNCHRONIZATION PROTOCOL

To start synchronization, the reference node, node 1, will send a sequence of m pulses that are d seconds apart. Since we assume the nodes have impulse radio transmitters, each pulse is extremely narrow in time. The values of d and m are parameters of the protocol that are established before deploying the network so the values are known by all nodes in the network. Therefore, in the time scale of node 1 the pulses are transmitted at times $\tau_0, \tau_0 + d, \dots, \tau_0 + d(m-1)$, where τ_0 is the time at which the synchronization process started. Let node 1 be the only element of the R_0 nodes.

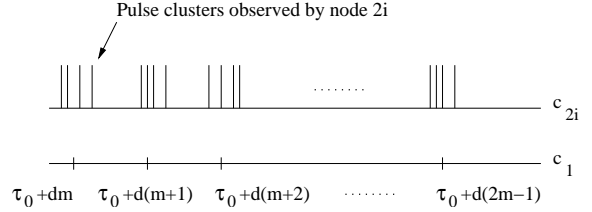


Fig. 3. A node $2i$ in R_2 has clock c_{2i} . This node will see clusters of pulse arrivals that are transmitted from a group of nodes in the set R_1 . These clusters arrive at node $2i$ around times $\tau_0 + dm, \tau_0 + d(m+1), \dots, \tau_0 + d(2m-1)$ in the time scale of node 1, c_1 .

The nodes that are in the broadcast domain of node 1 will hear this sequence of m pulses. We call these nodes the R_1 nodes and each node $i \in R_1, i \geq 1$, will be denoted by node $1i$. The vector of pulse arrival times observed by node $1i$ will be denoted \mathbf{Y}_{1i} . Each node $1i$ will be able to estimate its clock skew since it knows that node 1 transmitted these pulses d seconds apart. Each node $1i$ will also predict, in its own time scale, when times $\tau_0 + dm, \tau_0 + d(m+1), \dots, \tau_0 + d(2m-1)$ will occur in the time scale of node 1 and transmit m pulses, one at each predicted time. This means that each node $1i$ will transmit a pulse approximately at times $\tau_0 + dm, \tau_0 + d(m+1), \dots, \tau_0 + d(2m-1)$ in the time scale of node 1. When the R_1 nodes each transmit their sequence of m pulses, the nodes that can hear a subset of the R_1 nodes, the R_2 nodes, will observe clusters of pulses around the times $\tau_0 + dm, \tau_0 + d(m+1), \dots, \tau_0 + d(2m-1)$ since each node $2i$ can hear many R_1 nodes (Fig. 3). In fact, we make sure each node $2i$ can hear a cluster by requiring the node to observe at least \bar{N} pulses in each cluster. If a node $2i$ sees less than \bar{N} pulses in a cluster, then it will not make observations. Each node $2i$, a node $i \in R_2$, will note the arrival time of each pulse in the k th cluster, $k = 1, \dots, m$, and take the sample mean of these times to be its k th observation. Node $2i$'s vector of observations will be denoted as \mathbf{Y}_{2i} . Using these m observations, any node $2i$ will be able to estimate its clock skew since it knows that these observations should be occurring d seconds apart. As well, it will be able to predict in its local time scale when times $\tau_0 + d(2m), \tau_0 + d(2m+1), \dots, \tau_0 + d(3m-1)$ will occur in the time scale of the reference time. Node $2i$ will then transmit a pulse at each of those predicted times. This processes will repeat until all nodes in the network have an estimate of their clock skew. Notice that the R_1 nodes are not required to observe \bar{N} pulses in each cluster since they will always only receive a sequence of m pulses from node 1. Node

1 can simply broadcast a special packet to its surrounding nodes to identify the R_1 nodes. An illustration of the process can be found in Fig. 1 and note that nodes will remain silent for the remainder of the synchronization process after transmitting their m pulses. The cooperation occurs when a node ki in R_k , $k > 1$, can take a sample mean of a cluster of pulse arrivals.

To obtain the clock offset, the R_k nodes will broadcast a packet of information to the R_{k+1} nodes, $k \geq 0$. This packet will contain the value of τ_0 and a number q denoting the number of hops out from node 1. For example, node 1 will transmit the value of τ_0 and $q = 0$ to the R_1 nodes. The R_1 nodes will then send τ_0 and $q = 1$ to the R_2 nodes. In general, the R_k nodes will send τ_0 and $q = k$ to the R_{k+1} nodes. Any node ki will then know that its first observation approximately occurred at time $\tau_0 + dmq$ in the time scale of the reference time, where the value of q is the one received from set R_{k-1} .

We now describe how any node ki can estimate its clock skew, clock offset, and its m pulse transmission times. From (1), we know that there is a linear relationship between the reference clock c_1 and the clock of node ki , c_{ki} . Node ki will have a set of m observations denoted by the $m \times 1$ vector \mathbf{Y}_{ki} , where the elements of the vector are ordered from the earliest observation time to the latest observation time. Node ki will estimate its clock skew as

$$\hat{\alpha}_{ki} = \bar{\mathbf{C}}(\mathbf{H}^T \mathbf{H})^{-1} \mathbf{H}^T \mathbf{Y}_{ki} \quad (2)$$

and clock offset as

$$\hat{\Delta}_{ki} = \tilde{\mathbf{C}}(\mathbf{H}^T \mathbf{H})^{-1} \mathbf{H}^T \mathbf{Y}_{ki} - (\tau_0 + dm(k-1)), \quad (3)$$

where $\bar{\mathbf{C}} = [0 \ 1]$, $\tilde{\mathbf{C}} = [1 \ 0]$ and

$$\mathbf{H} = \begin{bmatrix} 1 & 1 & 1 & \dots & 1 \\ 0 & d & 2d & \dots & (m-1)d \end{bmatrix}^T \quad (4)$$

Note that in the calculation of the clock offset $\hat{\Delta}_{ki}$, the term $\tau_0 + dm(k-1)$ is the time in the time scale of c_1 that node ki should receive its first pulse. Node ki has used the τ_0 and $q = k-1$ parameters sent to it from the R_{k-1} nodes. Node ki will also estimate its own m pulse transmission times using

$$X_{ki}(l) = \mathbf{C}_l(\mathbf{H}^T \mathbf{H})^{-1} \mathbf{H}^T \mathbf{Y}_{ki}, \quad (5)$$

where $\mathbf{C}_l = [1 \ d(m+l)]$, for $l = 0, 1, \dots, m-1$. $X_{ki}(l)$ is the transmission time of node ki 's $(l+1)$ th pulse. A pseudo-code description is given in Table I. Note that the protocol described above is a completely new approach to the asymptotic spatial averaging ideas we studied in [17].

IV. TYPE I: BASIC COOPERATIVE NETWORKS

A. Network Setup

The most basic and fundamental deployment of nodes that effectively employs cooperative time synchronization is the case where *all* \bar{N} nodes at any given hop contribute to the signals observed at the next hop. This Type I deployment is illustrated in the top of Fig. 2 where each set of nodes R_i , $i \geq 1$, have \bar{N} nodes. We see that every node in R_i is in the broadcast domain of every node in R_{i-1} .

TABLE I

The synchronization protocol for each node ki , $k > 1$.

Cooperative Time Sync
wait for pulse arrivals, at least \bar{N} per cluster;
while (number of arrival clusters $< m$) {
record arrival time of all pulses;
listen for packet with τ_0 and q values;
};
for each (pulse arrival cluster j) {
$\mathbf{Y}_{ki}[j] =$ sample mean of cluster;
};
skew $\hat{\alpha}_{ki} = \bar{\mathbf{C}}(\mathbf{H}^T \mathbf{H})^{-1} \mathbf{H}^T \mathbf{Y}_{ki}$;
offset $\hat{\Delta}_{ki} = \tilde{\mathbf{C}}(\mathbf{H}^T \mathbf{H})^{-1} \mathbf{H}^T \mathbf{Y}_{ki} - (\tau_0 + dmq)$
for (1 from 0 to $m-1$) {
transmission time $X_{ki}(l) = \mathbf{C}_l(\mathbf{H}^T \mathbf{H})^{-1} \mathbf{H}^T \mathbf{Y}_{ki}$;
transmit pulse at $X_{ki}(l)$;
};
while (transmitting pulses) {
send a packet with values τ_0 and $q+1$;
};

B. Analysis

Due to the scalability problem, we would expect synchronization error to grow as timing information from node 1 (the R_0 node) is communicated to a node in the R_k set of nodes, $k > 0$. Therefore, it is of particular interest to quantify how the variance of the skew and offset estimates change as a function of the hop number k . Looking at the structure of the basic cooperative network in Fig. 2, we notice that the skew and offset estimates at a node ki must be dependent only on the estimates made by the nodes in R_{k-1} since all the information at R_k comes from the R_{k-1} set of nodes. Therefore, to understand the synchronization error growth over multiple hops, we need the distribution of the estimates made by the nodes in R_k as a function of the distribution of the estimates made by the nodes in R_{k-1} . Theorem 1, below, provides us with this characterization.

In the statement of the theorem we use e_l to be the column vector of all zeros except for a one in the l th position and

$$\bar{\mathbf{H}} = \begin{bmatrix} \mathbf{H} & 0 & \dots & 0 \\ 0 & \mathbf{H} & \dots & 0 \\ \vdots & \vdots & \ddots & \vdots \\ 0 & 0 & \dots & \mathbf{H} \end{bmatrix}, \quad (6)$$

where \mathbf{H} is from (4). Also, α_{ki} and $\bar{\Delta}_{ki}$ are the clock model parameters from (1) for node ki .

Theorem 1: Assume a Type I basic cooperative network.

(1) Given the distribution of the $2\bar{N} \times 1$ vector of estimates made by the R_{k-1} nodes,

$$\hat{\theta}_{k-1} \sim \mathcal{N}(\bar{\mu}_{k-1}, \bar{\Sigma}_{k-1}),$$

the distribution of the $2\bar{N} \times 1$ vector of estimates made by the R_k nodes,

$$\hat{\theta}_k \sim \mathcal{N}(\bar{\mu}_k, \bar{\Sigma}_k),$$

is found as follows: $\hat{\theta}_k$ has mean vector

$$\begin{aligned}\bar{\mu}_k &= E(\hat{\theta}_k) \\ &= E(\mathbf{A}_k \hat{\theta}_{k-1} + \mathbf{B}_k) \\ &= \mathbf{A}_k \bar{\mu}_{k-1} + \mathbf{B}_k \\ &= \begin{bmatrix} \alpha_{k1}(\tau_0 + (k-1)md - \bar{\Delta}_{k1}) \\ \alpha_{k1} \\ \vdots \\ \alpha_{k\bar{N}}(\tau_0 + (k-1)md - \bar{\Delta}_{k\bar{N}}) \\ \alpha_{k\bar{N}} \end{bmatrix}\end{aligned}\quad (7)$$

and covariance matrix

$$\bar{\Sigma}_k = \text{Cov}(\hat{\theta}_k) = \Sigma_{m_k} + \mathbf{A}_k \bar{\Sigma}_{k-1} \mathbf{A}_k^T \quad (8)$$

for

$$\Sigma_{m_k} = (\bar{\mathbf{H}}^T \bar{\mathbf{H}})^{-1} \bar{\mathbf{H}}^T \Sigma_{\bar{\mathbf{W}}_k} ((\bar{\mathbf{H}}^T \bar{\mathbf{H}})^{-1} \bar{\mathbf{H}}^T)^T$$

$$\Sigma_{\bar{\mathbf{W}}_k} = \mathbf{Q}_k \Sigma_{\bar{\Psi}_{k-1}} \mathbf{Q}_k^T + \sigma^2 \mathbf{I}_{\bar{N}m}$$

$$\mathbf{Q}_k = \begin{bmatrix} \alpha_{k1} \mathbf{I}_m \\ \vdots \\ \alpha_{k\bar{N}} \mathbf{I}_m \end{bmatrix}$$

$$\Sigma_{\bar{\Psi}_{k-1}} = \frac{\sigma^2}{\bar{N}^2} \sum_{i=1}^{\bar{N}} \frac{1}{\alpha_{(k-1)i}^2} \mathbf{I}_m$$

where

$$\mathbf{A}_k = \mathbf{D}_k \begin{bmatrix} \frac{1}{\alpha_{(k-1)1}} & \frac{dm}{\alpha_{(k-1)1}} & \cdots & 0 & 0 \\ 0 & \frac{1}{\alpha_{(k-1)1}} & \cdots & 0 & 0 \\ \vdots & \vdots & \ddots & \vdots & \vdots \\ 0 & 0 & \cdots & \frac{1}{\alpha_{(k-1)\bar{N}}} & \frac{dm}{\alpha_{(k-1)\bar{N}}} \\ 0 & 0 & \cdots & 0 & \frac{1}{\alpha_{(k-1)\bar{N}}} \end{bmatrix}$$

$$\mathbf{D}_k = \frac{1}{\bar{N}} \begin{bmatrix} \alpha_{k1} & 0 & \cdots & \alpha_{k1} & 0 \\ 0 & \alpha_{k1} & \cdots & 0 & \alpha_{k1} \\ \vdots & \vdots & \ddots & \vdots & \vdots \\ \alpha_{k\bar{N}} & 0 & \cdots & \alpha_{k\bar{N}} & 0 \\ 0 & \alpha_{k\bar{N}} & \cdots & 0 & \alpha_{k\bar{N}} \end{bmatrix}$$

$$\mathbf{B}_k = \mathbf{D}_k \begin{bmatrix} \bar{\Delta}_{(k-1)1} \\ 0 \\ \vdots \\ \bar{\Delta}_{(k-1)\bar{N}} \\ 0 \end{bmatrix} - \begin{bmatrix} \alpha_{k1} \bar{\Delta}_{k1} \\ 0 \\ \vdots \\ \alpha_{k\bar{N}} \bar{\Delta}_{k\bar{N}} \\ 0 \end{bmatrix}.$$

The initial conditions are

$$\bar{\mu}_1 = \begin{bmatrix} \alpha_{11}(\tau_0 - \bar{\Delta}_{11}) \\ \alpha_{11} \\ \vdots \\ \alpha_{1\bar{N}}(\tau_0 - \bar{\Delta}_{1\bar{N}}) \\ \alpha_{1\bar{N}} \end{bmatrix}$$

and $\bar{\Sigma}_1 = \sigma^2 (\bar{\mathbf{H}}^T \bar{\mathbf{H}})^{-1}$.

(2) The skew estimate and offset estimate for node ki can be found as

$$\hat{\alpha}_{ki} = e_{2(i-1)+2}^T \hat{\theta}_k \quad (9)$$

$$\hat{\Delta}_{ki} = e_{2(i-1)+1}^T \hat{\theta}_k - (\tau_0 + dm(k-1)) \quad (10)$$

for $i = 1, 2, \dots, \bar{N}$ and $k \geq 1$. \triangle

The proof of Theorem 1 is found in the appendix. Since the distribution of $\hat{\theta}_k$ is available, the distribution of $\hat{\alpha}_{ki}$ and $\hat{\Delta}_{ki}$ can be found. In fact, the variance of $\hat{\alpha}_{ki}$ can be found in element $(2(i-1)+2, 2(i-1)+2)$ of $\bar{\Sigma}_k$ in (8) and the variance of $\hat{\Delta}_{ki}$ can be found in element $(2(i-1)+1, 2(i-1)+1)$. The mean of $\hat{\alpha}_{ki}$ is the $(2(i-1)+2)$ th element of $\bar{\mu}_k$ in (7) and the mean of $\hat{\Delta}_{ki}$ can be found from the $(2(i-1)+1)$ th element shifted by $\tau_0 + dm(k-1)$.

From the statement of Theorem 1, we see that the distribution of the estimates made by the R_k nodes, $\hat{\theta}_k$, is completely determined from the distribution of $\hat{\theta}_{k-1}$. This recursive nature comes from the fact that the parameters estimated by the R_k nodes is only dependent on the estimates made by the R_{k-1} nodes. The relationship between $\hat{\theta}_{k-1}$ and $\hat{\theta}_k$ can be intuitively understood in two steps. First, $\hat{\theta}_{k-1}$ is the vector of synchronization parameters estimated by the nodes in R_{k-1} . Therefore, these estimates will establish the synchronization parameters for the R_k nodes since the R_{k-1} nodes communicate timing information to the R_k nodes. The synchronization parameters for R_k are found as

$$\bar{\theta}_k = \mathbf{A}_k \hat{\theta}_{k-1} + \mathbf{B}_k.$$

Second, the R_k nodes will use the timing information from the R_{k-1} nodes to make an unbiased estimate of the parameters $\bar{\theta}_k$, which gives us $\hat{\theta}_k$.

Since any node ki 's skew and offset estimates are found as affine transforms of $\hat{\theta}_k$ in (9) and (10), respectively, we see that any estimation errors made by the R_{k-1} nodes will be propagated to the R_k nodes' estimates of clock skew and clock offset. However, the intuitive understanding of cooperative time synchronization comes from realizing that the matrix \mathbf{A}_k takes an "average" over $\hat{\theta}_{k-1}$ thus mitigating the errors made by any particular node $(k-1)i$. As a result, the synchronization parameters communicated to the R_k nodes will be less noisy and, therefore, the skew and offset estimates made by a node ki will have less error. We would, thus, expect the variance of the estimates to decrease with increasing \bar{N} . Notice that our Type I network analysis does not explicitly utilize the circular transmission region with radius R .

C. Simulation Results

In Fig. 4 we illustrate the MATLAB simulation results for two 20 hop networks, one with $\bar{N} = 2$ and the other with $\bar{N} = 4$. The following parameters were used:

$$R = 1 \quad d = 5 \quad m = 4 \quad \sigma = 0.01$$

For each network, a set of $N = 20\bar{N} + 1$ nodes were first placed in a Type I network deployment. Each node's skew parameter was then generated using $\alpha_i = |X_i|$ for

$X_i \sim \mathcal{N}(1, 0.005)$, independently for each node i . Node 1 was assumed to have $\alpha_1 = 1$. The cooperative time synchronization protocol was then run 5000 times using the deployed network. At each hop, the 5000 skew and offset estimates of one chosen node were used to generate the simulated skew and offset estimate variance curves shown in Fig. 4. The theoretical variance value of the chosen node at each hop was computed using the recursive expression found in (8).

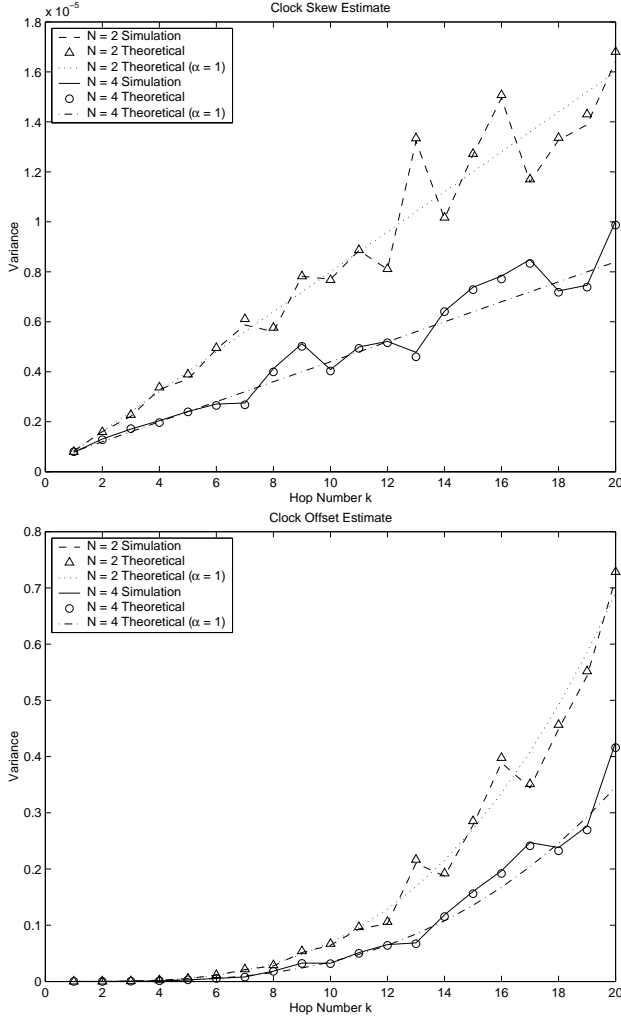


Fig. 4. $\text{Var}(\hat{\alpha}_{k1})$ is plotted in the top figure and $\text{Var}(\hat{\Delta}_{k1})$ is plotted in the bottom figure as a function of k .

In Fig. 4, we first clearly see that the simulated skew and offset variance values nicely match the predicted theoretical variance values. As well, the expected decrease in skew and offset variance as \bar{N} increases from 2 to 4 is immediately noticeable. In fact, in both the skew variance and offset variance curves, we have an approximate halving of the variance values as we double \bar{N} from 2 to 4. Also expected, is that the variance values at each hop depend on the particular values of α_i , $i = 1, \dots, N$. This dependence on the α_i values result in the jagged skew and offset variance curves seen in Fig. 4. The $\bar{N} = 2$ network had α_i values ranging from 0.9073 to 1.1342, while the $\bar{N} = 4$ network had skew values ranging from 0.8339 to 1.1669.

The problem with having the variance curves depend on the actual skew values is that the exact performance of cooperative time synchronization is dependent on the network realization. However, we find that for α_i values that are close to and centered around 1, the variance curves follow the trend established by the theoretical variance curves for $\alpha_i = 1$, all i . This can be seen in Fig. 4 where we have also plotted the theoretical curves using $\alpha_i = 1$ for all i for $\bar{N} = 2$ and $\bar{N} = 4$. As a result, the situation where $\alpha_i = 1$, all i , can be used to study the the performance improvement of cooperative time synchronization without dealing specifically with the skew values of individual nodes.

Therefore, to get a better understanding of how cooperative time synchronization improves synchronization performance, let us simplify the recursive expression in (8) for the special case where $\alpha_i = 1$ for all i and find a non-recursive expression for skew and offset variance. The first thing to note is that under the assumption of $\alpha_i = 1$ for all i , $\mathbf{A}_k = \mathbf{A}$ and $\Sigma_{m_k} = \Sigma_m$ are no longer dependent on k . Therefore, writing out the recursive expression for $\bar{\Sigma}_k$ (8), we have

$$\bar{\Sigma}_k = \sum_{i=0}^{k-2} \mathbf{A}^i \Sigma_m (\mathbf{A}^T)^i + \mathbf{A}^{k-1} \bar{\Sigma}_1 (\mathbf{A}^T)^{k-1}. \quad (11)$$

Using (11), Corollary 1 gives us the non-recursive expression for skew and offset variance.

Corollary 1: For a basic cooperative network with $\alpha_i = 1$, all i , $\hat{\alpha}_{ki}$ and $\hat{\Delta}_{ki}$ have the following mean and variance:

$$E(\hat{\alpha}_{ki}) = 1$$

$$E(\hat{\Delta}_{ki}) = -\bar{\Delta}_{ki}$$

$$\text{Var}(\hat{\alpha}_{ki}) = \frac{12\sigma^2}{d^2(m-1)m(m+1)} \left(1 + \frac{2(k-1)}{\bar{N}} \right) \quad (12)$$

$$\begin{aligned} \text{Var}(\hat{\Delta}_{ki}) = & \frac{2\sigma^2(2m-1)}{m(m+1)} + \frac{\sigma^2}{\bar{N}} \left[\frac{4(k-1)(2m-1)}{m(m+1)} \right. \\ & + (k-1)^2 \left(-\frac{12}{(m+1)} + \frac{12m}{(m-1)(m+1)} \right) \\ & \left. + \frac{1}{3}(k-2)(k-1)(2k-3) \frac{12m}{(m-1)(m+1)} \right] \quad (13) \end{aligned}$$

where k is a positive integer. \triangle

The proof of Corollary 1 is omitted since it is a direct simplification of (11). Note that the skew and offset variance expressions are only a function of k and not i . The theoretical skew and offset variance of the i th node at the k th hop (node ki) can be found in elements $(2(i-1)+2, 2(i-1)+2)$ and $(2(i-1)+1, 2(i-1)+1)$, respectively, of $\bar{\Sigma}_k$ in (11). However, the skew variance values in elements $(2(i-1)+2, 2(i-1)+2)$, $i = 1, \dots, \bar{N}$, are all equal and the offset variance values in elements $(2(i-1)+1, 2(i-1)+1)$, $i = 1, \dots, \bar{N}$, are also equal when we assume that $\alpha_i = 1$ for all i . As a result, we can consider the skew and offset variance at a hop k without specifying a particular node. Notice also that, besides the sign change in the mean of the offset estimate, the skew and offset

estimates are unbiased estimates of the clock parameters of node ki .

Looking at the skew and offset variance curves in (12) and (13), respectively, we see that the variance growth decreases like $1/\bar{N}$. This $1/\bar{N}$ factor in both (12) and (13) is expected since every node takes the sample mean of \bar{N} pulses to be an observation. The variance of the observation decreases like $1/\bar{N}$ because it is a sample mean and, thus, it is not surprising that the skew and offset variance values also approximately decrease like $1/\bar{N}$.

V. TYPE II: GENERAL NETWORKS

A. Network Setup

Nodes will not generally be clustered together as in a basic cooperative network, but be deployed in a more random manner. As a result, to study general network deployments, we will consider a Type II situation where nodes are uniformly deployed with density ρ over a circular region of radius LR with node 1 at the center. In such a setup, at any hop k , $k \geq 2$, a node ki in the R_k nodes will see *at least* \bar{N} nodes from the R_{k-1} set of nodes. However, the exact number of observed nodes will depend on node ki 's location in the region occupied by the R_k nodes.

An illustration of a Type II deployment is shown in Fig. 5. We note that the R_0 node (node 1) is placed at the center of the disk and the R_1 nodes occupy a circular region of radius R . However, the region occupied by the R_k nodes for $k \geq 2$ is a ring centered around node 1 with a ring thickness of $d_{max,k}$. For increasing k , the distance from node 1 to the inner circular boundary of the region occupied by the R_k set of nodes increases.

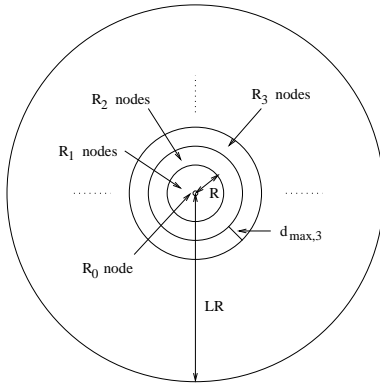


Fig. 5. A Type II network deployment. Nodes are deployed with uniform density ρ and node 1 is at the center of the network.

B. Analysis

To study a Type II network, we could carry out an analysis similar to the one we did for the Type I basic cooperative network. Assuming we know the location of all nodes for a given network deployment over the circular region of radius LR , we would be able to determine the neighbors of each node and then readily extend the Type I analysis to this Type II

network. The primary change that would occur in the analysis is the determination of the affine transform

$$\hat{\theta}_k \mapsto \bar{\theta}_{k+1} = \mathbf{A}_{k+1} \hat{\theta}_k + \mathbf{B}_{k+1}.$$

However, there are two issues that arise in determining the transform matrix \mathbf{A}_{k+1} and vector \mathbf{B}_{k+1} .

First, since R_k and R_{k+1} will most likely have different numbers of nodes, we immediately see that \mathbf{A}_{k+1} will be a $2|R_{k+1}| \times 2|R_k|$ matrix and \mathbf{B}_{k+1} will be a $2|R_{k+1}| \times 1$ vector, where $|R_k|$ is the cardinality of set R_k . This means that the length of vector $\hat{\theta}_k$ will change with every hop.

Second, for any node $(k+1)i$ in R_{k+1} , the set of cooperating nodes in R_k will be different. Thus, \mathbf{A}_k will also reflect this difference. Therefore, every time we move from hop k to $k+1$, the correlation structure of $\hat{\theta}_k$ will change.

Together, these two points suggest that even though it is possible to carry out the full analysis, the complexity would make the resulting expressions depend on the particular network realization and not provide significant insight into the problem. In fact, it would be nearly impossible to visualize the result without carrying out a numerical evaluation. Since our goal is to comprehend the impact of spatial averaging on general networks, we choose to proceed directly with simulations and compare the results with our analytical expressions for Type I networks.

In the following analysis, we develop a basic understanding of what we would expect to see in the simulation results that are presented in Section V-C. We assume that the number of nodes in any given area of the Type II network is proportional to the area. The reason is that for uniformly deployed nodes with density ρ , the average number of nodes in an area \mathcal{A} is $\mathcal{A}\rho$. Note that even though the analysis and simulation results for Type II networks use the assumption of a circular transmission range of R , the simulation results in Section V-C still provide valid insight when realistic transmission regions [15], [16] are assumed since the figures illustrate synchronization error as a function of *hop* number. Therefore, regardless of the shape of the transmission region, a node at hop k will have received the appropriate synchronization information and, thus, our simulation results reflect its synchronization performance.

1) *Estimation of \bar{L}* : Our first consideration is to estimate the number of hops, \bar{L} , required to communicate timing information from node 1 to the edge of the network a distance LR away. In order to do this, we need a way to quantify $d_{max,k}$. In Fig. 6, we illustrate $d_{max,2}$ and see that $d_{max,2}$ is determined by having the intersection of the two radius R circles contain an average of \bar{N} nodes. This is because if we increase $d_{max,2}$, then nodes at this increased distance will not see \bar{N} nodes on average and, thus, not be considered an R_2 node. However, $d_{max,k} > d_{max,2}$, for $k > 2$, because the ring occupied by the R_k nodes increases in size for increasing k . As a result, we choose to be conservative and let $d_{max} \triangleq d_{max,2}$ approximate $d_{max,k}$ for all k . This means that our estimate of \bar{L} using d_{max} will be greater than or equal to the number of hops required to reach a distance of LR when the differences in $d_{max,k}$ are considered.

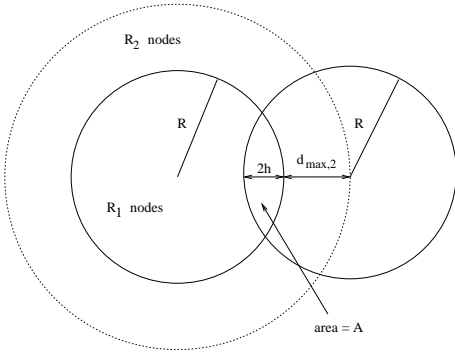


Fig. 6. An illustration of $d_{max,2}$.

Let A be the area of the intersection of the two radius R circles in Fig. 6 and we have from [18] that

$$A = 2 \left(R^2 \cos^{-1} \left(\frac{R-h}{R} \right) - (R-h) \sqrt{2Rh-h^2} \right). \quad (14)$$

Since A contains \bar{N} nodes, we have that

$$A = \bar{N}/\rho. \quad (15)$$

From (14) and (15) we can numerically determine h thus giving us

$$d_{max} = R - 2h. \quad (16)$$

As a result, we need \bar{L} to satisfy

$$R + (\bar{L} - 1)d_{max} \geq LR$$

which means that

$$\bar{L} = \left\lceil \frac{R(L-1)}{R-2h} + 1 \right\rceil. \quad (17)$$

2) *Comparison to Type I Networks:* We will compare the Type II network simulation results to the Type I analytical results. This comparison will allow us to carry over the intuition regarding spatial averaging that we have developed for the basic cooperative network. However, Type I and Type II networks differ primarily in that Type I networks assume that all nodes will observe \bar{N} neighbors from the previous hop while any node in a Type II network will only see *at least* \bar{N} nodes. Thus, if we want to compare Type I and Type II plots, we need to establish some meaningful choices of the number of cooperating nodes for use with expressions (12) and (13).

Looking at (a) of Fig. 7, we see that if a node ki in the region occupied by the R_k nodes is at the circular boundary farthest from node 1 (outer circular boundary), then it will likely hear only \bar{N} nodes from R_{k-1} . That is, there are $\bar{N} = A_1\rho$ nodes in area A_1 . Recall that \bar{N} is the minimum number of R_{k-1} nodes any node ki will hear. However, looking at (b) in Fig. 7, a node ki at the circular boundary closest to node 1 (inner circular boundary) in the R_k region will hear many more nodes. In fact, a node ki at the boundary between R_{k-1} and R_k will hear the largest average number of nodes $\bar{N}_{max}(k) = A_2\rho$. Since \bar{N} and $\bar{N}_{max}(k)$ is the range of the number of cooperating nodes seen by a node in R_k , it would make sense to plot Type I expressions (12) and (13) using these two values. However, $\bar{N}_{max}(k)$ varies with k . In Fig. 8

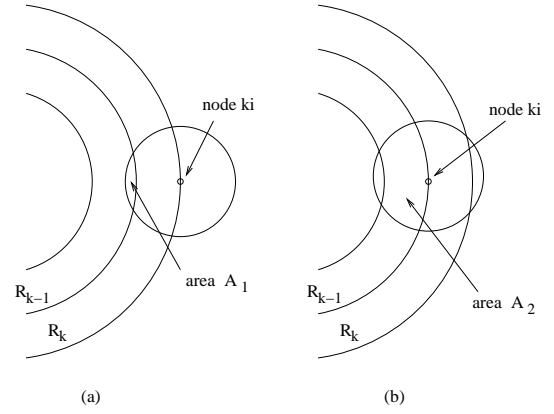


Fig. 7. (a) Node ki at the outer circular boundary of the R_k set of nodes. (b) Node ki at the inner circular boundary of the R_k set.

we illustrate the regions occupied by the R_k nodes for $k = 1$, $k > 1$, and $k \gg 1$ overlaid on top of each other and in each situation, we see that the set of nodes in R_k seen by a node at the boundary between the R_k nodes and the R_{k+1} nodes is different for changing values of k . However, it is clear that the area of intersection always falls inside a semicircle of radius R . As a result, we will approximate $\bar{N}_{max} = \max_{k:k \geq 2} \bar{N}_{max}(k)$, by upper bounding the maximum area of intersection with the area of the semicircle. This means that

$$\bar{N}_{max} \approx \rho \frac{\pi R^2}{2}. \quad (18)$$

Thus, in comparing Type II and Type I results, we will use \bar{N} and \bar{N}_{max} in (18) with both (12) and (13)

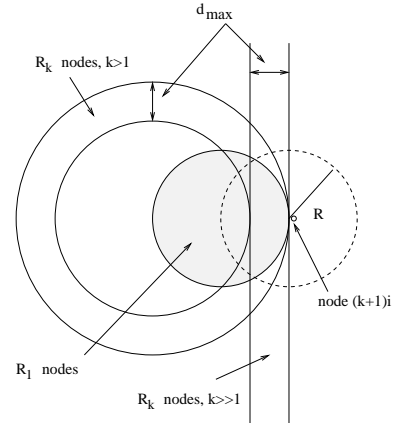


Fig. 8. The regions occupied by the R_k nodes for $k = 1$, $k > 1$, and $k \gg 1$ overlaid on top of each other. The region of nodes seen by a node at the inner circular boundary of R_{k+1} changes with k .

Using \bar{N} with (12) and (13) will provide a curve that tends to be higher than the Type II simulated curves for two main reasons. First, since \bar{N} is the minimum number of nodes in R_{k-1} that a node ki in R_k will hear and we know that a larger number of cooperating nodes will result in decreased estimation variance, the variance values computed using \bar{N} will tend to be higher. Second, even if a node ki in R_k hears \bar{N} nodes from R_{k-1} , each of those \bar{N} nodes did not necessarily only hear \bar{N} nodes from R_{k-2} . Thus, the skew and offset

estimates made by each of those \bar{N} nodes in R_{k-1} whose transmissions are being heard by node ki may have a variance that is less than predicted by (12) and (13) using \bar{N} . The improved skew and offset estimates made by the nodes in R_{k-1} will thus lead to a lower estimation variance for node ki even though node ki hears only \bar{N} from R_{k-1} .

Using \bar{N}_{max} with (12) and (13) will provide a curve that tends to be lower than the Type II simulated curves for two similar reasons. First, since \bar{N}_{max} is the average number of nodes heard by a node at the inner circular boundary of R_k , $k \geq 2$, and all other nodes in R_k will on average hear fewer nodes, a Type I curve using \bar{N}_{max} will tend to yield lower values. Second, not all nodes in R_{k-1} make their estimates using a signal cooperatively generated by \bar{N}_{max} nodes. In fact, most nodes in R_{k-1} observe fewer than \bar{N}_{max} nodes. As a result, the lower quality estimates made by some of the R_{k-1} nodes will cause the estimation variance of the R_k nodes that hear \bar{N}_{max} from R_{k-1} to be greater than predicted by (12) and (13) using \bar{N}_{max} .

3) *Synchronization Performance and Node Density*: The third issue we want to address in analyzing a Type II network deployment is how to decrease synchronization error when we know from Section V-B.1 that the number of hops \bar{L} required to communicate timing information from node 1 to the edge of the network a distance LR away is determined by \bar{N} . Given a fixed R , we can start with some \bar{N} and ρ . Using (14), (15), and (16), we can determine the value of d_{max} and, hence, from (17) the number of hops \bar{L} required to send timing information from node 1 to the edge of the network. In order to decrease synchronization error at a distance LR from node 1, we need to increase \bar{N} . However, only increasing \bar{N} will decrease d_{max} and increase \bar{L} . Therefore, we need to increase both \bar{N} and ρ . From (14) and (15), we see that if \bar{N}/ρ is kept constant, then h will be constant. If h is constant, then so is d_{max} . As a result, by increasing node density, we can increase the minimum number of cooperating nodes \bar{N} and therefore decrease synchronization error.

C. Simulation Results

In the following simulation results, we have assumed that all nodes in the network have no clock skew, i.e. $\alpha_i = 1$ for all i . From Section IV-C we know that general α_i values result in variance curves that follow the trends established by curves generated using $\alpha_i = 1$. As a result, using $\alpha_i = 1$ for all i allows us to study the benefits of spatial averaging without considering effects that are dependent on the particular network realization.

1) *Comparison to Type I Results*: To being the study of cooperative time synchronization in general networks, we deploy a network for Simulation 1 with the parameters in Table II. The simulation results are displayed in Fig. 9. In each run, a new network of nodes was uniformly deployed over a circular area of radius $LR = 5$ and the MATLAB simulator implemented the cooperative time synchronization protocol. Besides plotting the Type I comparison curves described in Section V-B.2, we also plot the sample variance of the best performing node and the worse performing node. In each

TABLE II
Simulation 1 Parameters

ρ	19.10
\bar{N}	4
R	1
L	5
d	2
m	4
σ	0.01
Number of Runs	5000

run, the node in R_k that sees the fewest number of nodes from R_{k-1} is considered the worse performing node while the node in R_k that sees the largest number of nodes from R_{k-1} is the best performing node. For the l th run, the fewest number of nodes seen by a node in R_k is denoted $X_{min}^{(l)}(k)$ while the largest number of nodes seen by a node in R_k is denoted $X_{max}^{(l)}(k)$. The skew and offset estimate of the best and worst performing node at each hop is recorded and the sample variance over the 5000 runs is plotted.

The top figure in Fig. 9 illustrates the sample skew variance curves of the worst and best synchronized node along with the Type I curves for comparison. The bottom figure in Fig. 9 illustrates the clock offset estimate sample variance. Note that using equation (17) and the parameters in Table II, we find that $\bar{L} = 7$. From the simulations, we also see that 7 hops are required to traverse the network. In fact, only 7.32% of the networks required more than 7 hops to reach all nodes in the network.

As predicted in Section V-B.2, we clearly see in Fig. 9 that the worst case variance and the best case variance are sandwiched between the Type I comparison curves. Also, as expected, the skew and offset variances do not closely follow the upper and lower Type I comparison curves. The worst case skew and offset variance follow the upper comparison curve for the first 2 hops and then begin to deviate from the curve. As mentioned in Section V-B.2, this is because the nodes contributing to the worst performing node may have received signals from more than \bar{N} nodes. Similarly, the best case skew and offset variance follow the lower comparison curve for the first 2 hops before deviating. This is because many of the nodes contributing signals to the best performing node made their estimates using a signal cooperatively generated by less than \bar{N}_{max} nodes. Also of interest is the steep decrease in the worst case skew and offset variance at hop $k = 7$. This is due to the fact that on average, the distance from the outer circular boundary of the R_6 region to the network boundary is much less than d_{max} . As a result, the R_7 region is smaller and $X_{min}(7)$ will be larger than \bar{N} . Table III shows the $X_{min}(k) = \frac{1}{5000} \sum_{l=1}^{5000} X_{min}^{(l)}(k)$ and $X_{max}(k) = \frac{1}{5000} \sum_{l=1}^{5000} X_{max}^{(l)}(k)$ values and we see that $X_{min}(6) = \bar{N} = 4$, but $X_{min}(7)$ is nearly twice $X_{min}(6)$.

We also note that $X_{max}(k)$ increases from 27.56 for $k = 2$ to 35.32 for $k = 7$. Using (18), however, we find that $\bar{N}_{max} = 30$. The reason $X_{max}(k)$ increases with each hop and does not equal \bar{N}_{max} is because $X_{max}(k)$ is a different statistic. \bar{N}_{max} approximates the average number of R_{k-1} nodes seen by a node ki at the inner circular boundary of R_k . However,

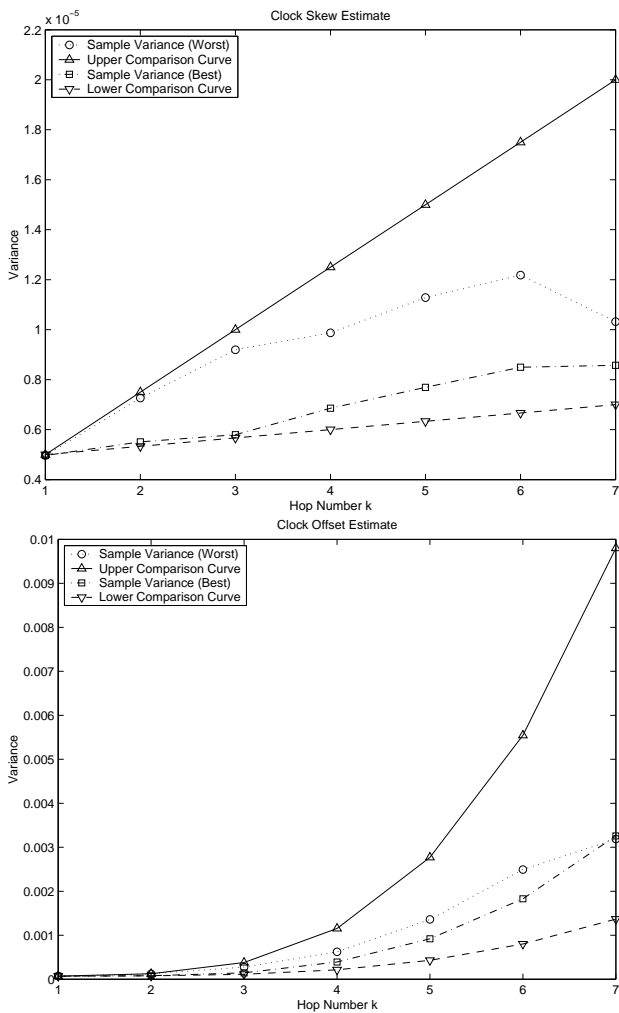


Fig. 9. Simulation 1. Top: Sample variance for the skew estimate of a Type II network along with Type I comparison curves. Bottom: Sample variance of the offset estimate along with Type I comparison curves.

TABLE III
 $X_{min}(k)$ and $X_{max}(k)$ for Fig. 9

k	$X_{min}(k)$	$X_{max}(k)$
1	1	1
2	4.00	27.56
3	4.00	29.36
4	4.00	31.86
5	4.00	33.50
6	4.00	34.60
7	7.77	35.32

$X_{max}^{(l)}(k)$ is the largest number of nodes seen by any node ki in R_k for the l th network realization. Therefore, $X_{max}^{(l)}(k)$ is actually an ordered statistic since it takes the largest number of nodes seen by a node at hop k . $X_{max}(k)$ is thus the mean of the ordered statistic. Therefore, we would not expect \bar{N}_{max} and $X_{max}(k)$ to be the same. Also, $X_{max}(k)$ increases with k since as the circumference of the circular ring occupied by R_k increases, there are more nodes at the boundary between R_k and R_{k-1} . Since there are more nodes at the boundary, there are also more opportunities to find the largest number

of nodes seen by a node ki . Thus, the maximum number of nodes would tend to be larger. Note that, not considering the effects at the network boundary, $X_{min}(k) = \bar{N}$ because the definition of the protocol specifies the minimum to be \bar{N} and there is little randomness in determining $X_{min}(k)$.

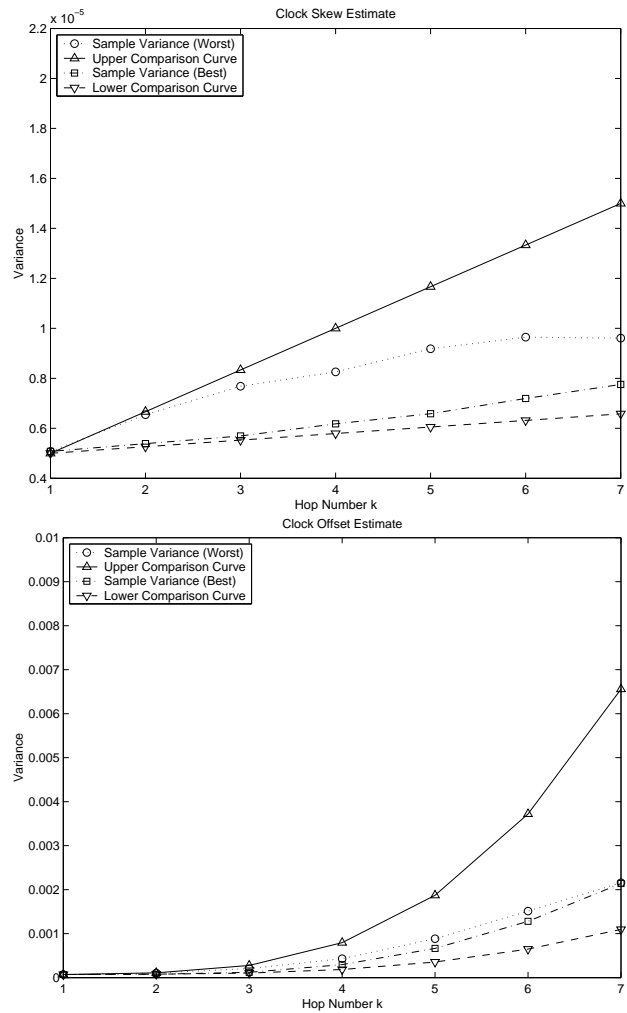


Fig. 10. Simulation 1b. The Type I comparison curves and the Type II sample skew and offset variance curves are lower as compared to Fig. 9 when \bar{N} and ρ are increased. More cooperation yields improved synchronization performance.

TABLE IV
Simulation 1b Parameters

ρ	23.87
\bar{N}	6
R	1
L	5
d	2
m	4
σ	0.01
Number of Runs	5000

2) *Synchronization Performance and Node Density*: Next, we want to improve synchronization performance by increasing node density. Starting with the parameters for Simulation 1, we increase the minimum number of cooperating nodes

to $\bar{N} = 6$ while keeping $\bar{N}/\rho = 0.25$ constant. Therefore, for Simulation 1b (Table IV), $\rho = 23.87$ and we plot the simulation results in Fig. 10. Comparing Fig. 9 and Fig. 10, it is clear that Fig. 10 yields improved skew and offset variances, thus showing that increased node density and larger \bar{N} values indeed improve synchronization performance in Type II networks. In Table V we show $X_{min}(k)$ and $X_{max}(k)$ for Fig. 10. Note that there is only a slight decrease in the worst case skew and offset variance curves at hop $k = 7$ since in this simulation, we have that $X_{min}(7) = 6.57$ is only slightly larger than $X_{min}(6) = \bar{N} = 6$.

TABLE V
 $X_{min}(k)$ and $X_{max}(k)$ for Fig. 10

k	$X_{min}(k)$	$X_{max}(k)$
1	1	1
2	6.00	34.01
3	6.00	34.64
4	6.00	37.64
5	6.00	39.50
6	6.00	40.80
7	6.57	41.70

Another very effective way to visualize how increasing ρ and \bar{N} can decrease skew and offset variance is to choose one *test node* in the network and consider how its skew and offset variance decreases as the network density and number of cooperating nodes are increased. In Simulation 2 (Table VI), we placed a test node at distance $LR = 2.2$ from node 1 and simulated its skew and offset variance as we increased ρ and \bar{N} . \bar{N} took on values ranging from 1 to 10 and we adjusted ρ accordingly to keep $\bar{N}/\rho = 0.15$ fixed. The results are plotted in Fig. 11 and we clearly see that as \bar{N} increases along with ρ , the skew and offset variance of this test node decreases. Also, from Section V-B.3, we know that since we keep \bar{N}/ρ constant, the number of hops required to reach the test node stays the same as we increase \bar{N} . Therefore, since the test node is at $\bar{L} = 3$ for every value of \bar{N} , we have also plotted the upper and lower Type I comparison curves for the skew and offset variance at hop $k = 3$ to illustrate how the comparison curves change in relation to the simulated variance curves. In Fig. 11, the simulated skew and offset variance curves of the test node fall between the Type I upper and lower comparison curves.

TABLE VI
Simulation 2 Parameters

\bar{N}/ρ	0.15
\bar{N}	[1 2 4 6 8 10]
R	1
L	2.2
d	1
m	2
σ	0.01
Number of Runs	5000

It is clear that by keeping the ratio \bar{N}/ρ constant while increasing \bar{N} and ρ allows us to reduce the synchronization error at each hop while keeping the number of hops required to synchronize the network, \bar{L} , constant. The variance of the skew

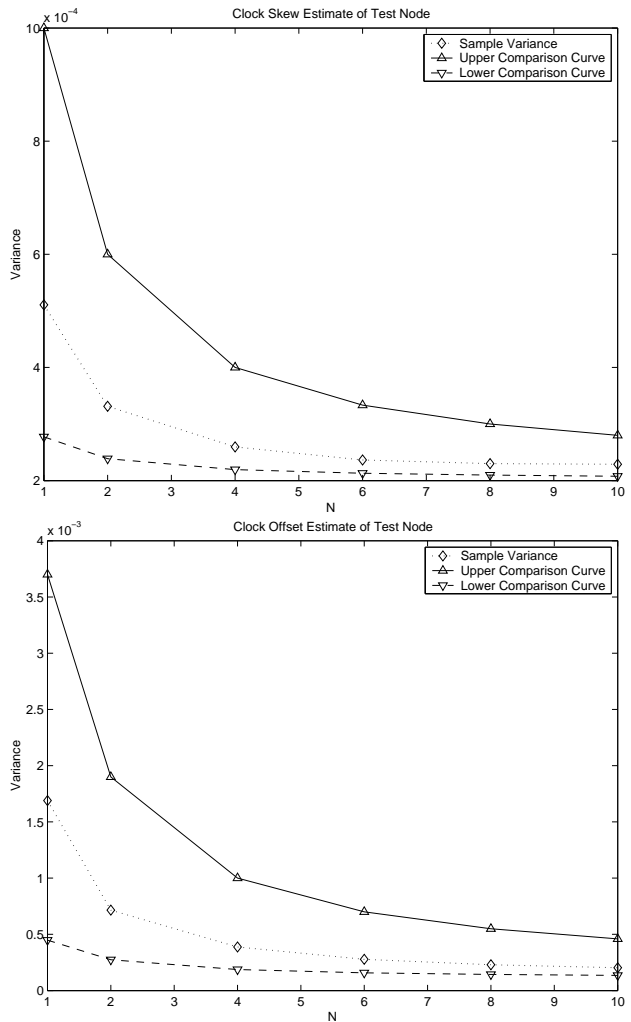


Fig. 11. Simulation 2. Variance of the skew and offset estimates of the test node fall between the Type I comparison curves and decrease with increasing \bar{N} and ρ .

and offset estimates is decreased by increasing the minimum number of cooperating nodes.

Furthermore, from the simulations in this section, we find that the upper and lower Type I comparison curves provide a good reference to the performance of Type II networks. We have established that the best and worst case variance values for the Type II skew and offset estimates fall between the upper and lower Type I comparison curves. As the density of the network and \bar{N} are both increased, the comparison curves will shift downwards and become closer together. Thus, we would expect the variance of the Type II network estimates to change similarly with increasing \bar{N} and ρ .

VI. CONCLUSION

In this paper we have proposed one technique that uses spatial averaging in dense networks as a means to improving global time synchronization. Spatial averaging is used to improve the timing data points that are used to estimate clock skew and clock offset. By decreasing the error in the timing data points, improved clock skew and clock offset

estimates can be made. Our analysis of the technique in a basic cooperative network revealed that the error variance in both the clock skew and clock offset estimates can be significantly decreased as the number of cooperating nodes increases. Simulation results also show that synchronization over large, multi-hop networks can be improved by increasing node density. Further analysis and a comparison between cooperative and non-cooperative techniques can be found in [19].

This scalable protocol provides an alternate way to combat the scalability problem. It allows us to simply increase the number of nodes in the network to obtain improved synchronization performance. The new trade-off between network density and synchronization performance provided by spatial averaging will allow for added flexibility in designing future networks.

It is important to note that the concept of spatial averaging is very general and our proposed cooperative technique is but one manner in which to take advantage of it. Our protocol shows that techniques using spatial averaging can be designed. Even though the proposed protocol has certain limitations, such as requiring access to the physical layer, it allows us to successfully illustrate the performance improvement achievable using spatial averaging. Future work will focus on other approaches to spatial averaging. For example, it would be desirable to develop a cooperative technique using spatial averaging that achieves performance gains while needing only access to the data link or network layer.

APPENDIX

Proof of Theorem 1 Node 1 begins the synchronization processes by transmitting a sequence of pulses at times $\tau_0 + ld$, for $l = 0, \dots, m-1$. For simplicity, assume that τ_0 and d are integer values. Note that since node 1 transmits these pulses in its own time scale c_1 (the reference time), the pulses will occur at integer values of t . Using the clock model in (1), any node $1i$, $i = 1, \dots, \bar{N}$, in the R_1 set of nodes will get a vector of observations \mathbf{Y}_{1i} , where $\mathbf{Y}_{1i}[1] = \alpha_{1i}(\tau_0 - \bar{\Delta}_{1i}) + \Psi_{1i,1}$ and the $(l+1)$ th element of \mathbf{Y}_{1i} is $\mathbf{Y}_{1i}[l+1] = \alpha_{1i}(\tau_0 - \bar{\Delta}_{1i}) + ld\alpha_{1i} + \Psi_{1i,l+1}$. This can also be written as

$$\mathbf{Y}_{1i} = \mathbf{H}\theta_{1i} + \mathbf{W}_{1i}, \quad (19)$$

where

$$\theta_{1i} = \begin{bmatrix} \theta_{1i,1} \\ \theta_{1i,2} \end{bmatrix} = \begin{bmatrix} \alpha_{1i}(\tau_0 - \bar{\Delta}_{1i}) \\ \alpha_{1i} \end{bmatrix}$$

with \mathbf{H} as in (4) and $\mathbf{W}_{1i} = [W_{1i,1}, \dots, W_{1i,m}]^T$. Since $\Psi_{1i,l+1}$ is an independent Gaussian random variable for each l , $\mathbf{W}_{1i} \sim \mathcal{N}(0, \Sigma_{1i})$ with $\Sigma_{1i} = \sigma^2 \mathbf{I}_m$. As mentioned, this set of observations is for any node $1i$ in the set of R_1 nodes.

Since we have \bar{N} R_1 nodes, we can write the vector of observations made by all R_1 nodes as

$$\bar{\mathbf{Y}}_1 = \bar{\mathbf{H}}\bar{\theta}_1 + \bar{\mathbf{W}}_1 \quad (20)$$

where

$$\bar{\mathbf{Y}}_1 = \begin{bmatrix} \mathbf{Y}_{11} \\ \vdots \\ \mathbf{Y}_{1\bar{N}} \end{bmatrix}, \quad \bar{\theta}_1 = \begin{bmatrix} \theta_{11} \\ \vdots \\ \theta_{1\bar{N}} \end{bmatrix}, \quad \bar{\mathbf{W}}_1 = \begin{bmatrix} \mathbf{W}_{11} \\ \vdots \\ \mathbf{W}_{1\bar{N}} \end{bmatrix}$$

and $\bar{\mathbf{H}}$ is as in (6). Note that $\bar{\mathbf{W}}_1 \sim \mathcal{N}(0, \sigma^2 \mathbf{I}_{\bar{N}m})$. This way we have $\bar{\mathbf{Y}}_1$ as the vector of observations made by all R_1 nodes and we can make a UMVU (uniformly minimum variance unbiased) estimate of $\bar{\theta}_1$ by taking

$$\hat{\bar{\theta}}_1 = (\bar{\mathbf{H}}^T \bar{\mathbf{H}})^{-1} \bar{\mathbf{H}}^T \bar{\mathbf{Y}}_1 \sim \mathcal{N}(\bar{\mu}_1, \bar{\Sigma}_1),$$

where

$$\bar{\mu}_1 = \bar{\theta}_1, \quad \bar{\Sigma}_1 = \sigma^2 (\bar{\mathbf{H}}^T \bar{\mathbf{H}})^{-1}.$$

It is easy to see that

$$(\bar{\mathbf{H}}^T \bar{\mathbf{H}})^{-1} = \begin{bmatrix} (\mathbf{H}^T \mathbf{H})^{-1} & \dots & 0 \\ \vdots & \ddots & \vdots \\ 0 & \dots & (\mathbf{H}^T \mathbf{H})^{-1} \end{bmatrix}$$

and

$$(\mathbf{H}^T \mathbf{H})^{-1} = \begin{bmatrix} \frac{2(2m-1)}{m(m+1)} & \frac{-6}{dm(m+1)} \\ \frac{-6}{dm(m+1)} & \frac{12}{d^2(m-1)m(m+1)} \end{bmatrix}.$$

This establishes the initial conditions for the theorem. $\hat{\bar{\theta}}_1$ is a $2\bar{N} \times 1$ column vector where the subvector made up of the $(2(i-1)+1)$ th and $(2(i-1)+2)$ th elements, $i = 1, \dots, \bar{N}$, is $\hat{\theta}_{1i} = (\mathbf{H}^T \mathbf{H})^{-1} \mathbf{H}^T \mathbf{Y}_{1i}$. Therefore, any node $1i$'s skew estimate (2) and offset estimate (3) can be found from $\hat{\bar{\theta}}_1$ as

$$\hat{\alpha}_{1i} = e_{2(i-1)+2}^T \hat{\bar{\theta}}_1 \quad (21)$$

and

$$\hat{\Delta}_{1i} = e_{2(i-1)+1}^T \hat{\bar{\theta}}_1 - \tau_0 \quad (22)$$

where e_l is the column vector of all zeros except for a one in the l th position.

Each node $1i$ can now make an estimate of the next appropriate integer value of t , in this case $t = \tau_0 + md$, by making a minimum variance unbiased estimate of $\theta_{1i,1} + md\theta_{1i,2} = \alpha_{1i}(\tau_0 - \bar{\Delta}_{1i}) + md\alpha_{1i}$. This can be done with the estimator

$$\hat{\tau}_{1i} = \hat{\theta}_{1i,1} + md\hat{\theta}_{1i,2} = \mathbf{C}_0 \hat{\theta}_{1i}$$

where $\mathbf{C}_0 = [1 \quad md]$. This will then be node $1i$'s estimate of the next appropriate integer value of t in its own time scale c_{1i} .

From (5), every node $1i$ will then transmit a sequence of m pulses occurring, in the time scale of c_{1i} , at $X_{1i}(l) = \hat{\tau}_{1i} + ld\hat{\theta}_{1i,2}$, for $l = 0, \dots, m-1$. Using the clock model (1), we find that in the time scale of c_1 these pulses occur at

$$\begin{aligned} (\hat{\tau}_{1i} + ld\hat{\theta}_{1i,2})_{c_1} &= \frac{\hat{\tau}_{1i} + ld\hat{\theta}_{1i,2} - \Psi_{1i,l+1}}{\alpha_{1i}} + \bar{\Delta}_{1i} \\ &= \frac{\hat{\tau}_{1i}}{\alpha_{1i}} + \bar{\Delta}_{1i} + ld \frac{\hat{\theta}_{1i,2}}{\alpha_{1i}} - \frac{\Psi_{1i,l+1}}{\alpha_{1i}}. \end{aligned}$$

Any node $2j$ in the R_2 set of nodes that can hear node $1i$ will thus get a sequence of pulses

$$\begin{aligned} \tilde{\mathbf{Y}}_{2j}[l+1] &= \alpha_{2j} \left(\left(\frac{\hat{\tau}_{1i}}{\alpha_{1i}} + \bar{\Delta}_{1i} + ld \frac{\hat{\theta}_{1i,2}}{\alpha_{1i}} - \frac{\Psi_{1i,l+1}}{\alpha_{1i}} \right) - \bar{\Delta}_{2j} \right) \\ &\quad + \Psi_{2j,l+1}, \end{aligned}$$

where $l = 0, \dots, m-1$.

In this Type I network deployment every node $2j$ hears the same set of \bar{N} nodes and takes the sample mean of each cluster of pulses for its observation, we can express the actual vector of observations made by node $2j$ as

$$\begin{aligned} \mathbf{Y}_{2j}[l+1] &= \sum_{i=1}^{\bar{N}} \frac{\alpha_{2j}}{\bar{N}} \left(\left(\frac{\hat{\tau}_{1i}}{\alpha_{1i}} + \bar{\Delta}_{1i} + ld \frac{\hat{\theta}_{1i,2}}{\alpha_{1i}} - \frac{\Psi_{1i,l+1}}{\alpha_{1i}} \right) - \bar{\Delta}_{2j} \right) \\ &\quad + \Psi_{2j,l+1}, \end{aligned}$$

where $l = 0, \dots, m-1$. Note that since these pulse arrivals are clustered, we assume that for a given cluster, each pulse arrival is corrupted by the same jitter. Thus, receiver side jitter $\Psi_{2j,l+1}$ is an independent sample for every l , but takes the same value for each i . This models the fact that clock errors occurring in a small time window are highly correlated while errors farther apart in time are independent. We can rewrite this simply as $\mathbf{Y}_{2j}[l+1] = \alpha_{2j}((\tau_1 + ld\tilde{\alpha}_1 - \tilde{\Psi}_{1,l+1}) - \bar{\Delta}_{2j}) + \Psi_{2j,l+1}$, where

$$\begin{aligned} \tau_1 &\triangleq \frac{1}{\bar{N}} \sum_{i=1}^{\bar{N}} \frac{\hat{\tau}_{1i}}{\alpha_{1i}} + \bar{\Delta}_{1i} & \tilde{\alpha}_1 &\triangleq \frac{1}{\bar{N}} \sum_{i=1}^{\bar{N}} \frac{\hat{\theta}_{1i,2}}{\alpha_{1i}} \\ \tilde{\Psi}_{1,l+1} &\triangleq \frac{1}{\bar{N}} \sum_{i=1}^{\bar{N}} \frac{\Psi_{1i,l+1}}{\alpha_{1i}}. \end{aligned}$$

Since every node $2j$ will see the same \bar{N} , this means that every node $2j$ will have the same τ_1 and $\tilde{\alpha}_1$. Therefore, τ_1 and $\tilde{\alpha}_1$ are now fixed, and it can be easily found that

$$\begin{bmatrix} \tilde{\Psi}_{1,1} \\ \vdots \\ \tilde{\Psi}_{1,m} \end{bmatrix} \sim \mathcal{N}\left(0, \Sigma_{\tilde{\Psi}_1}\right)$$

where

$$\Sigma_{\tilde{\Psi}_1} = \frac{\sigma^2}{\bar{N}^2} \sum_{i=1}^{\bar{N}} \frac{1}{\alpha_{1i}^2} \mathbf{I}_m.$$

Node $2j$'s vector of observations can also be written in a linear form similar to (19), $\mathbf{Y}_{2j} = \mathbf{H}\theta_{2j} + \mathbf{W}_{2j}$, where

$$\theta_{2j} = \begin{bmatrix} \theta_{2j,1} \\ \theta_{2j,2} \end{bmatrix} = \begin{bmatrix} \alpha_{2j}(\tau_1 - \bar{\Delta}_{2j}) \\ \alpha_{2j}\tilde{\alpha}_1 \end{bmatrix}$$

with \mathbf{H} as in (4) and $\mathbf{W}_{2j} = [W_{2j,1} \dots W_{2j,m}]^T$.

$$\mathbf{W}_{2j} = \alpha_{2j} \begin{bmatrix} \tilde{\Psi}_{1,1} \\ \vdots \\ \tilde{\Psi}_{1,m} \end{bmatrix} + \begin{bmatrix} \Psi_{2j,1} \\ \vdots \\ \Psi_{2j,m} \end{bmatrix} \sim \mathcal{N}(0, \Sigma_{2j})$$

with

$$\Sigma_{2j} = \sigma^2 \left(1 + \frac{\alpha_{2j}^2}{\bar{N}^2} \sum_{i=1}^{\bar{N}} \frac{1}{\alpha_{1i}^2} \right) \mathbf{I}_m.$$

The vector of observations made by all R_2 nodes can be written in a manner similar to (20),

$$\bar{\mathbf{Y}}_2 = \bar{\mathbf{H}}\bar{\theta}_2 + \bar{\mathbf{W}}_2$$

where

$$\begin{aligned} \bar{\mathbf{Y}}_2 &= \begin{bmatrix} \mathbf{Y}_{21} \\ \vdots \\ \mathbf{Y}_{2\bar{N}} \end{bmatrix}, \quad \bar{\theta}_2 = \begin{bmatrix} \theta_{21} \\ \vdots \\ \theta_{2\bar{N}} \end{bmatrix}, \quad \mathbf{Q}_2 = \begin{bmatrix} \alpha_{21} \mathbf{I}_m \\ \vdots \\ \alpha_{2\bar{N}} \mathbf{I}_m \end{bmatrix} \\ \bar{\mathbf{W}}_2 &= \begin{bmatrix} \mathbf{W}_{21} \\ \mathbf{W}_{22} \\ \vdots \\ \mathbf{W}_{2\bar{N}} \end{bmatrix} = \mathbf{Q}_2 \begin{bmatrix} \tilde{\Psi}_{1,1} \\ \vdots \\ \tilde{\Psi}_{1,m} \end{bmatrix} + \begin{bmatrix} \Psi_{21,1} \\ \vdots \\ \Psi_{21,m} \\ \vdots \\ \Psi_{2\bar{N},1} \\ \vdots \\ \Psi_{2\bar{N},m} \end{bmatrix} \end{aligned}$$

This means that $\bar{\mathbf{W}}_2 \sim \mathcal{N}(0, \Sigma_{\bar{\mathbf{W}}_2})$, where

$$\Sigma_{\bar{\mathbf{W}}_2} = \mathbf{Q}_2 \Sigma_{\tilde{\Psi}_1} \mathbf{Q}_2^T + \sigma^2 \mathbf{I}_{\bar{N}m}.$$

The R_2 nodes will estimate $\bar{\theta}_2$ as

$$\begin{aligned} \hat{\bar{\theta}}_2 &= (\bar{\mathbf{H}}^T \bar{\mathbf{H}})^{-1} \bar{\mathbf{H}}^T \bar{\mathbf{Y}}_2 \\ &\sim \mathcal{N}(\bar{\theta}_2, (\bar{\mathbf{H}}^T \bar{\mathbf{H}})^{-1} \bar{\mathbf{H}}^T \Sigma_{\bar{\mathbf{W}}_2} ((\bar{\mathbf{H}}^T \bar{\mathbf{H}})^{-1} \bar{\mathbf{H}}^T)^T). \end{aligned} \quad (23)$$

However, for analysis, this does not give us the complete distribution of $\hat{\bar{\theta}}_2$ since $\bar{\theta}_2$ is a function of $\hat{\theta}_1$. Therefore, we first consider how θ_{2j} is a function of $\hat{\theta}_1$. We find that

$$\begin{aligned} \theta_{2j} &= \begin{bmatrix} \alpha_{2j}(\tau_1 - \bar{\Delta}_{2j}) \\ \alpha_{2j}\tilde{\alpha}_1 \end{bmatrix} \\ &= \begin{bmatrix} \alpha_{2j} \left(\frac{1}{\bar{N}} \sum_{i=1}^{\bar{N}} \frac{\hat{\tau}_{1i}}{\alpha_{1i}} + \bar{\Delta}_{1i} - \bar{\Delta}_{2j} \right) \\ \alpha_{2j} \frac{1}{\bar{N}} \sum_{i=1}^{\bar{N}} \frac{\hat{\theta}_{1i,2}}{\alpha_{1i}} \end{bmatrix} \\ &= \begin{bmatrix} \alpha_{2j} \left(\frac{1}{\bar{N}} \sum_{i=1}^{\bar{N}} \frac{\hat{\theta}_{1i,1} + md\hat{\theta}_{1i,2}}{\alpha_{1i}} + \bar{\Delta}_{1i} - \bar{\Delta}_{2j} \right) \\ \alpha_{2j} \frac{1}{\bar{N}} \sum_{i=1}^{\bar{N}} \frac{\hat{\theta}_{1i,2}}{\alpha_{1i}} \end{bmatrix} \\ &= \frac{\alpha_{2j}}{\bar{N}} \sum_{i=1}^{\bar{N}} \left(\begin{bmatrix} \frac{1}{\alpha_{1i}} & \frac{dm}{\alpha_{1i}} \\ 0 & \frac{1}{\alpha_{1i}} \end{bmatrix} \begin{bmatrix} \hat{\theta}_{1i,1} \\ \hat{\theta}_{1i,2} \end{bmatrix} \right) \\ &\quad + \begin{bmatrix} \bar{\Delta}_{1i} \\ 0 \end{bmatrix} \Big) - \alpha_{2j} \begin{bmatrix} \bar{\Delta}_{2j} \\ 0 \end{bmatrix} \end{aligned} \quad (24)$$

Using (24) we have

$$\bar{\theta}_2 = \mathbf{A}_2 \hat{\theta}_1 + \mathbf{B}_2, \quad (25)$$

where

$$\mathbf{A}_2 = \mathbf{D}_2 \begin{bmatrix} \frac{1}{\alpha_{11}} & \frac{dm}{\alpha_{11}} & \dots & 0 & 0 \\ 0 & \frac{1}{\alpha_{11}} & \dots & 0 & 0 \\ \vdots & \vdots & \ddots & \vdots & \vdots \\ 0 & 0 & \dots & \frac{1}{\alpha_{1\bar{N}}} & \frac{dm}{\alpha_{1\bar{N}}} \\ 0 & 0 & \dots & 0 & \frac{1}{\alpha_{1\bar{N}}} \end{bmatrix},$$

$$\mathbf{B}_2 = \mathbf{D}_2 \begin{bmatrix} \bar{\Delta}_{11} \\ 0 \\ \vdots \\ \bar{\Delta}_{1\bar{N}} \\ 0 \end{bmatrix} - \begin{bmatrix} \alpha_{21} \bar{\Delta}_{21} \\ 0 \\ \vdots \\ \alpha_{2\bar{N}} \bar{\Delta}_{2\bar{N}} \\ 0 \end{bmatrix},$$

for

$$\mathbf{D}_2 = \frac{1}{\bar{N}} \begin{bmatrix} \alpha_{21} & 0 & \dots & \alpha_{21} & 0 \\ 0 & \alpha_{21} & \dots & 0 & \alpha_{21} \\ \vdots & \vdots & \ddots & \vdots & \vdots \\ \alpha_{2\bar{N}} & 0 & \dots & \alpha_{2\bar{N}} & 0 \\ 0 & \alpha_{2\bar{N}} & \dots & 0 & \alpha_{2\bar{N}} \end{bmatrix}.$$

Using (23) and (25), the distribution of $\hat{\theta}_2$ can now be found.

$$\begin{aligned} \bar{\mu}_2 &= E(\hat{\theta}_2) \\ &= E(E(\hat{\theta}_2|\hat{\theta}_1)) \\ &= E(\bar{\theta}_2) \\ &= E(\mathbf{A}_2\hat{\theta}_1 + \mathbf{B}_2) \\ &= \begin{bmatrix} \alpha_{21}(\tau_0 + md - \bar{\Delta}_{21}) \\ \alpha_{21} \\ \vdots \\ \alpha_{2\bar{N}}(\tau_0 + md - \bar{\Delta}_{2\bar{N}}) \\ \alpha_{2\bar{N}} \end{bmatrix} \end{aligned} \quad (26)$$

Using the decomposition

$$\text{Cov}(\hat{\theta}_2) = E(\text{Cov}(\hat{\theta}_2|\hat{\theta}_1)) + \text{Cov}(E(\hat{\theta}_2|\hat{\theta}_1)),$$

we have from (23) and (25)

$$\begin{aligned} \Sigma_{m_2} &= E(\text{Cov}(\hat{\theta}_2|\hat{\theta}_1)) \\ &= (\bar{\mathbf{H}}^T \bar{\mathbf{H}})^{-1} \bar{\mathbf{H}}^T \Sigma_{\bar{\mathbf{W}}_2} ((\bar{\mathbf{H}}^T \bar{\mathbf{H}})^{-1} \bar{\mathbf{H}}^T)^T \end{aligned}$$

$$\begin{aligned} \text{Cov}(E(\hat{\theta}_2|\hat{\theta}_1)) &= \text{Cov}(\bar{\theta}_2) \\ &= \mathbf{A}_2 \bar{\Sigma}_1 \mathbf{A}_2^T, \end{aligned}$$

giving us

$$\bar{\Sigma}_2 = \text{Cov}(\hat{\theta}_2) = \Sigma_{m_2} + \mathbf{A}_2 \bar{\Sigma}_1 \mathbf{A}_2^T. \quad (27)$$

Thus, the distribution of $\hat{\theta}_2$ is

$$\hat{\theta}_2 \sim \mathcal{N}(\bar{\mu}_2, \bar{\Sigma}_2).$$

$\hat{\theta}_2$ is again a $2\bar{N} \times 1$ column vector where the subvector made up of the $(2(i-1)+1)$ th and $(2(i-1)+2)$ th elements, $i = 1, \dots, \bar{N}$, is $\hat{\theta}_{2i} = (\mathbf{H}^T \mathbf{H})^{-1} \mathbf{H}^T \mathbf{Y}_{2i}$. Therefore, as in (21) and (22), any node $2i$'s skew estimate (2) and offset estimate (3) can be found from $\hat{\theta}_2$ as

$$\hat{\alpha}_{2i} = e_{2(i-1)+2}^T \hat{\theta}_2 \quad (28)$$

and

$$\hat{\Delta}_{2i} = e_{2(i-1)+1}^T \hat{\theta}_2 - (\tau_0 + dm). \quad (29)$$

Each node $2i$ will now be able to transmit a sequence of m pulses occurring, in the time scale of c_{2i} , at $X_{2i}(l) = \hat{\tau}_{2i} + ld\hat{\theta}_{2i,2}$, for $l = 0, \dots, m-1$, where $\hat{\tau}_{2i} = \hat{\theta}_{2i,1} + md\hat{\theta}_{2i,2}$. Repeating the same process we carried out for the observations of any node $2j$ with any node $3j$, we can find $\hat{\theta}_3 \sim \mathcal{N}(\bar{\mu}_3, \bar{\Sigma}_3)$. In fact, continuing this procedure, we can find the distribution of $\hat{\theta}_k$ for the R_k nodes as

$$\hat{\theta}_k \sim \mathcal{N}(\bar{\mu}_k, \bar{\Sigma}_k)$$

where similar to (26) we have $\bar{\mu}_k = E(\hat{\theta}_k)$ which is found in (7) and similar to (27) we have

$$\bar{\Sigma}_k = \text{Cov}(\hat{\theta}_k) = \Sigma_{m_k} + \mathbf{A}_k \bar{\Sigma}_{k-1} \mathbf{A}_k^T,$$

which is found in (8). Σ_{m_k} , \mathbf{A}_k , \mathbf{B}_k , and $\Sigma_{\bar{\mathbf{W}}_k}$ are as in the theorem statement. As in (28) and (29), any node ki 's skew estimate (2) and offset estimate (3) can be found from $\hat{\theta}_k$ as

$$\hat{\alpha}_{ki} = e_{2(i-1)+2}^T \hat{\theta}_k$$

and

$$\hat{\Delta}_{ki} = e_{2(i-1)+1}^T \hat{\theta}_k - (\tau_0 + dm(k-1)).$$

This concludes the proof of Theorem 1. \triangle

REFERENCES

- [1] J. Elson, L. Girod, and D. Estrin. Fine-Grained Network Time Synchronization using Reference Broadcasts. In *Proc. 5th Symp. Op. Syst. Design Implementation (OSDI)*, Boston, MA, 2002.
- [2] M. L. Sichitiu and C. Veerarittiphan. Simple, Accurate Time Synchronization for Wireless Sensor Networks. In *Proc. IEEE Wireless Communication and Networking Conference (WCNC 2003)*, New Orleans, LA, March 2003.
- [3] S. Ganeriwal, R. Kumar and M. B. Srivastava. Timing-Sync Protocol for Sensor Networks. In *Proc. First ACM Conference on Embedded Networked Sensor Systems (SenSys)*, Los Angeles, CA, November 2003.
- [4] J. van Greunen and J. Rabaey. Lightweight Time Synchronization for Sensor Networks. In *Proc. 2nd ACM International Workshop on Wireless Sensor Networks and Applications (WSNA 2003)*, San Diego, CA, September 2003.
- [5] M. Maroti, B. Kusy, G. Simon and A. Ledeczi. The Flooding Time Synchronization Protocol. In *Proc. 2nd International Conference on Embedded Networked Sensor Systems*, Baltimore, MD, November 2004.
- [6] C. Kelly IV, V. Ekanayake, and R. Manohar. SNAP: A Sensor Network Asynchronous Processor. In *Proc. 9th Int. Symp. Async. Circ. Syst.*, Vancouver, BC, 2003.
- [7] B. Warneke, M. Last, B. Liebowitz, and K. S. J. Pister. Smart Dust: Communicating with a Cubic-Millimeter Computer. *IEEE Computer Mag.*, 34(1):44–51, 2001.
- [8] H. Li, A. Lal, J. Blanchard, and D. Henderson. Self-Reciprocating Radioisotope-Powered Cantilever. *J. Applied Phys.*, 92(2):1122–1127, 2002.
- [9] R. E. Mirolo and S. H. Strogatz. Synchronization of Pulse-Coupled Biological Oscillators. *SIAM J. Appl. Math.*, 50(6):1645–1662, 1990.
- [10] D. Lucarelli and I. Wang. Decentralized Synchronization Protocols with Nearest Neighbor Communication. In *Proc. SenSys'04*, Baltimore, Maryland, 2004.
- [11] Y. Hong and A. Scaglione. A Scalable Synchronization Protocol for Large Scale Sensor Networks and its Applications. *IEEE Journal on Selected Areas in Communications (JSAC)*, 23(5):1085–1099, May 2005.
- [12] G. Werner-Allen, G. Tewari, A. Patel, M. Welsh, and R. Nagpal. Firefly-Inspired Sensor Network Synchronicity with Realistic Radio Effects. In *Proc. SenSys'05*, San Diego, CA, November 2005.
- [13] A. Hu and S. D. Servetto. Cooperative Time Synchronization with Propagation Delay: Model and Analysis. In *Proc. 43rd Annual Allerton Conference on Communication, Control, and Computing*, Monticello, IL, October 2005.
- [14] A. Hu and S. D. Servetto. On the Scalability of Cooperative Time Synchronization in Pulse-Connected Networks. *IEEE Transactions on Information Theory*, 52(6):2725–2748, 2006.
- [15] D. Ganesan, B. Krishnamachari, A. Woo, D. Culler, D. Estrin and S. Wicker. Complex Behavior at Scale: An Experimental Study of Low-Power Wireless Sensor Networks. In *Technical Report UCLA/CSD-TR 02-0013*, Computer Science Department, UCLA, July 2002.
- [16] J. Zhao and R. Govindan. Understanding Packet Delivery Performance in Dense Wireless Sensor Networks. In *Proc. 1st International Conf. on Embedded Networked Sensor Systems*, Los Angeles, CA, 2003.
- [17] A. Hu and S. D. Servetto. Algorithmic Aspects of the Time Synchronization Problem in Large-Scale Sensor Networks. *ACM/Kluwer Mobile Networks and Applications. Special Issue on Wireless Sensor Networks*. 10:491-503, 2005.

- [18] E. W. Weisstein. Circular Segment. From *MathWorld*—A Wolfram Web Resource. <http://mathworld.wolfram.com/CircularSegment.html>
- [19] A. Hu. Cooperative Time Synchronization Using Spatial Averaging Ph.D. Thesis, Cornell University, January 2007.